Tribo-design of lubricants for power loss reduction in the oil-film bearings of a process industry machine: modelling and experimental tests

Steven Chatterton[a]*, Paolo Pennacchi[a], Andrea Vania[a], Andrea De Luca[b], Phuoc Vinh Dang[c]

[a] Politecnico di Milano, Department of Mechanical Engineering Via La Masa 1, 20156 Milano, Italy
[b] Danieli & C Officine Meccaniche S.p.A., Research & Development, Via Nazionale 41, 33042 Buttrio (UD), Italy
[c] Department of Mechanical Engineering, The University of Danang-University of Science and Technology, 54, Nguyen Luong Bang Street, Danang, Viet Nam

Abstract. This paper addresses the optimization of the tribological characteristics of lubricating oils used in the process industry. In many cases, the machines are organized in several “stands” to form “lines” and are equipped by spindles supported by oil-film journal bearings that are fed by the same oil. The modelling of a steel roll forming line is presented by using a thermo-elasto-hydro-dynamic model for the calculation of the power dissipated in each journal bearing. The optimal lubricating oil characteristics are defined by means of a multivariate optimization on the parameters of viscosity, temperature and thickness of the oil-film. The results of the experimental tests are shown for the oil used in the real plant and the new oil formulated by simulations.

Keywords: Power loss, Power saving, Lubricants, Viscosity, Journal bearings, Tribology.

* Corresponding author: steven.chatterton@polimi.it

1 Introduction

Oil-film journal bearings are still widely employed in industry because of their simplicity and low cost in high-load or high-speed applications [1-6]. Typical applications in the process industry are represented by machines with medium/large diameter shafts, even operating at low Sommerfeld numbers [7], and characterized by both low tangential speeds and high loads. Conversely, other applications, such as in power generation or in the oil & gas fields, can be characterized by high speeds and low loads.
In this paper, the case of a steel roll forming machine equipped with several oil-film journal bearings [7-9] operating in different conditions is considered.

Steel roll forming is a continuous process for forming sheet, strip, or coiled metal stock into long shapes of uniform cross-section. The material passes through multiple pairs of contoured rolls that progressively form the workpiece to meet the desired specifications [10]. Roll forming machines typically have a number of dual-spindle roll forming stands, where two counter-rotating rolls or wheels are used to obtain the desired cross section shape in each stand. Roll-forming technology belongs to the nonlinear problem of large plastic deformation, and finite element method theory is usually employed for the estimation of stresses and deformations in the workpiece and the forming forces involved in the process [11]. As the cross-section decreases from the inlet of the material to the outlet of the forming machine, the length of the workpiece will change (see Fig. 1a). The first stands have lower speeds, whereas the last stands usually have high rotational speeds.

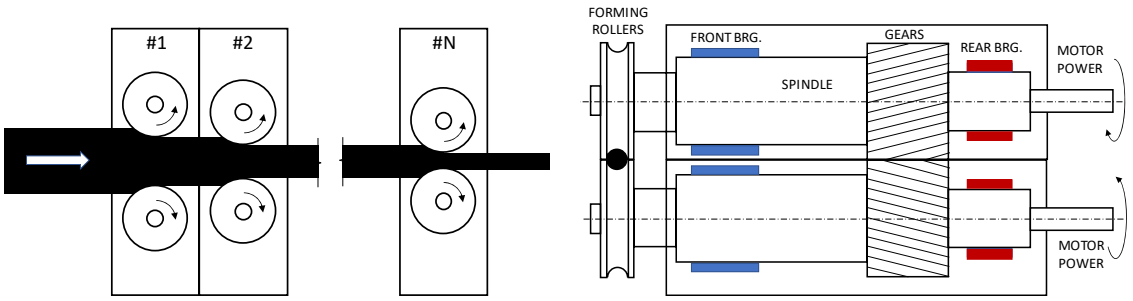

a) b)

Fig. 1. a) Example of a steel roll forming machine and b) arrangement of each stand.

Power losses in oil-film journal bearings are usually neglected in the field of process industry. In the literature, several papers address the reduction of power loss in oil-film journal bearings, especially in the case of automotive engines [12, 13, 14, 15]. Allmaier et al. in [16] accurately investigates the friction in journal bearings of automotive engines by considering the friction due to metallic asperity contact between sliding surfaces in mixed lubricated regime. Experimental results for different lubricants on a test-rig are compared with elasto-hydrodynamic calculations in [16] and thermo-elasto-hydrodynamic calculations in [17]. Models for the asperity contact friction in mixed lubrication conditions are well summarized in [18].

Reduction of power losses due to mechanical friction can be obtained by reducing the oil viscosity [19, 20] or by modifying the surface topography with textures and the material of the mating surfaces.

Grützmacher et al. in [21] proves the reduction of power losses in mixed lubrication regime by adding surface patterns on the shaft of journal bearings. Murthy and

Raghunandana in [22] investigate the effect of dimples on journal bearing bushing to reduce the friction using Taguchi method. Kalogiannis in [23] investigates, by simulations and experiments, the power loss reduction in the bearings of a diesel engine crankshaft by adopting polymer coated bearings. Wei et al. in [24] study the effect of dimensional tolerances on the power loss for a journal bearing.

A lot of literature deals with tribological properties of oil additives for friction reduction. Simmons and Glavatskih in [25] investigate higher viscosity index lubricants with lower viscosity base oil by experiments on a full-scale journal bearing test rig. Nanoparticles have been used by Gulzar et al. in [26] as lubricant additive. Marx et al. in [27] investigate by experiments the dependence of the viscosity on the shear rate for several blends of base oil with viscosity modifier additives and detergent-inhibitor package.

In this paper, the modelling of the steel roll forming line is presented by using a TEHD (thermo-elasto-hydro-dynamic) model for the calculation of the power dissipated in each journal bearing [28-30].

The detailed analysis of the behaviour of all the bearings in the machines has been reported, by considering the mineral oil commonly used in steel roll forming machines, referred to in the following as the reference oil.

Then, the optimized dynamic viscosity curve of the oil that reduce the overall power loss is obtained and can be used for the formulation of a new oil.

The results of the experimental activity performed by means of a test rig are reported. In the experimental tests, two different oils are investigated: the first is the current one used in the real plant, and the second is a new oil formulated to obtain the viscosity designed by the simulations.

For reasons of confidentiality, some data of the forming machine and the results of simulations have been normalized with respect to the maximum values obtained in the investigation.

2 Description of the steel roll forming machine

The steel roll forming machine considered in the paper is composed by $N = 10$ equal stands with increasing rotational speed. Each stand is composed of two spindles in parallel configuration rotating at the same speed in opposite direction, as shown in Fig. 1b. The rotational speed of the spindles is also synchronized by two gears.

Each spindle is supported by two oil-film plain journal bearings, namely, the front and the rear one. The rear bearing is smaller than the front one. All the stands are equal and equipped with the same components to reduce the number of spare parts. This dynamic allows the costs of maintenance operations to be reduced and allows the flexibility of the machine to be increased by adding or removing stands in the machine depending on the workpiece to be produced. In general, the use of too few passes can cause loss of tolerance, whereas the use of too many passes increases the final tooling cost.

The rotational speed and load in each stand are shown in Fig. 2. As previously stated, for confidentiality reasons, the rotational speed in each stand has been normalized with respect to the maximum rotational speed of the last stand and the estimated load on the bearings with respect to the maximum load obtained in the front bearing of the first stand. For example, the speed in the last stand is approximately 5 times the speed in the first stand, and the load in the rear bearing of the last stand is approximately 25 times lower than the load in the front bearing of the first stand. The loads have been calculated by the machine manufacturer by modelling the steel forming process.

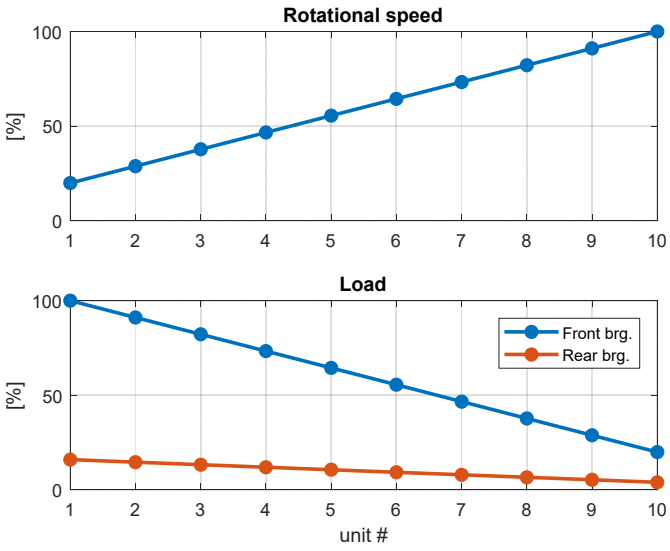

Fig. 2. Operating speed and load of the bearings.

3 Bearing model

The bearings supporting the spindle have the shape shown in Fig. 3; each bearing is characterized by two axial grooves located in the unloaded part [7]. An additional groove in the circumferential direction is in the middle of the bearing and connects the two axial grooves. The oil enters from the inlet hole and fills all the grooves during the shaft rotation. The bearing mainly consists of a base steel part with a layer of anti-friction alloy in the inner surface.

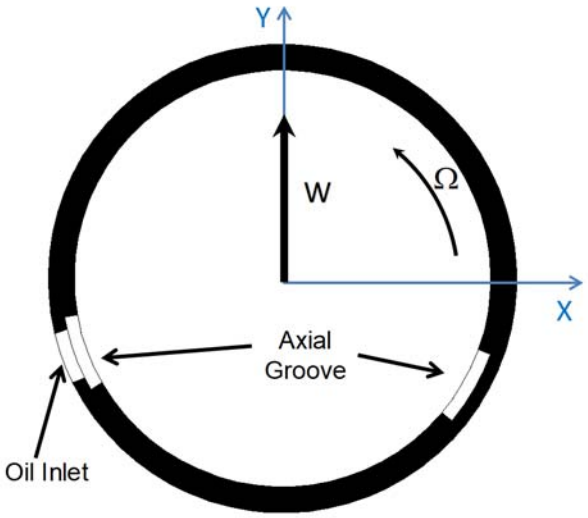

Fig. 3. Simplified drawing of the bearing installed in the steel forming machine, with the load directed upwards.

For the sake of simplicity, the load shown in Fig. 3 is assumed to be in the vertical direction only, even if in the real application it is composed of the two components in the perpendicular and tangential directions with respect to the direction of the roll forming process (see Fig. 1). The bearings in the real machine have an angular configuration that accommodates the actual average direction of the load. In this paper, the configuration of all the bearings is the same, and an average value of the real load direction in the stands is assumed for all the bearings of the model.

The TEHD model of the bearing includes the laws of hydrodynamic lubrication, the thermal effect due to shear stresses in the oil-film and the deformation of the bearing due to mechanical and thermal stresses.

For a given static load, the following conditions must be satisfied:

- convergence of the pressure distribution in the oil-film;
- convergence of the temperature distribution in the system;
- convergence of bearing deformation;
- equilibrium of the forces on the shaft.

The simulation code was developed by the authors based on Matlab®. The optimization toolbox was used for solving the equilibrium position of the system, the partial differential equation toolbox was used for solving the three-dimensional thermal model for the temperature distribution, and the three-dimensional structural-mechanics model was used for the bearing deformation.

3.1 Hydrodynamic problem

The hydrodynamic part of the model is based on the well-known Reynolds equation (see, for example, [3,4,6]):

$$\frac{\partial}{\partial x}\left(\frac{\rho h^3}{12\mu}\frac{\partial p}{\partial x}\right)+\frac{\partial}{\partial z}\left(\frac{\rho h^3}{12\mu}\frac{\partial p}{\partial z}\right)=\frac{\partial}{\partial x}\left(\frac{\rho h U}{2}\right)-\rho V \tag{1}$$

where x is the tangential direction, z is the axial direction, h is the oil-film thickness, p is the pressure, μ is the dynamic viscosity and U, V represent the velocity terms in the tangential and radial directions of the shaft, respectively.

3.2 Cavitation problem

The cavitation problem has been solved on the basis of the algorithm presented by Giacopini et al. in [33] that uses the “complementarity concept” and ensures the mass conservation. In the active (non cavitated) region, the fluid density ρ is constant and

equal to ρ_0. In the cavitated (non-active) region, the density becomes lower because of the presence of vapor and gas bubbles. In contrast, the pressure has a complementary behaviour. The pressure is zero in the cavitated region, whereas it has a greater value in the other parts of oil bearing. If pressure p is multiplied by $(\rho_0 - \rho)$, then the Reynolds equation can be rewritten as a complementary problem in the complementary variables p and r:

$$\begin{cases} \dfrac{\partial}{\partial x}\left(\dfrac{h^3}{k_x \mu}\dfrac{\partial p}{\partial x}\right)+\dfrac{\partial}{\partial z}\left(\dfrac{h^3}{k_z \mu}\dfrac{\partial p}{\partial z}\right)=-\dfrac{\partial}{\partial x}\left(\dfrac{rhU}{2}\right)+\dfrac{\partial}{\partial x}\left(\dfrac{hU}{2}\right)+V(r-1) \\ p \geq 0 \\ r=\dfrac{\rho_0-\rho}{\rho_0} \geq 0 \\ p \cdot r = 0 \end{cases} \tag{2}$$

where k_x and k_z are turbulent flow coefficients that will be described in the next section.

The solution of eq. (2) can be obtained using the finite different method. By discretizing the derivatives in eq. (6) on the grid, it is possible to obtain the pressure $p_{i,j}$ and the complementary variable $r_{i,j}$ at node (i,j) of the mesh grid as a combination of corresponding values of adjacent nodes:

$$\begin{aligned} &a_1\, p_{i+1,j} + a_2\, p_{i\text{-}1,j} + a_3\, p_{i,j+1} + a_4\, p_{i,j\text{-}1} + a_5\, p_{i,j} + \\ &\quad + b_1\, r_{i+1,j} + b_2\, r_{i\text{-}1,j} + b_3\, r_{i,j+1} + b_4\, r_{i,j\text{-}1} + b_5\, r_{i,j} + c = 0 \end{aligned} \tag{3}$$

By considering all the nodes of the mesh grid, it is possible to obtain a linear system as follows:

$$[A]\mathbf{p}+[B]\mathbf{r}+\mathbf{c}=0 \tag{4}$$

where $\mathbf{p}$ is the column vector that contains the value of pressure for all the nodes of the grid domain used in the finite-difference method. Vectors $\mathbf{p}$ and $\mathbf{r}$ include unknown values $\mathbf{p}_u$ and $\mathbf{r}_u$ respectively, to be evaluated, and known values $\mathbf{p}_k$ and $\mathbf{r}_k$ are given by the boundary conditions (zero pressure or known density at boundaries) or by the supplied pressure in correspondence of the grooves. Therefore, it is necessary to rearrange eq. (4) as follows:

$$\begin{bmatrix} A_{kk} & A_{ku} \\ A_{uk} & A_{uu} \end{bmatrix} \begin{Bmatrix} \mathbf{p}_k \\ \mathbf{p}_u \end{Bmatrix} + \begin{bmatrix} B_{kk} & B_{ku} \\ B_{uk} & B_{uu} \end{bmatrix} \begin{Bmatrix} \mathbf{r}_k \\ \mathbf{r}_u \end{Bmatrix} + \begin{Bmatrix} \mathbf{c}_k \\ \mathbf{c}_u \end{Bmatrix} = 0 \tag{5}$$

Thus, the solution of complementary problem in the unknown variables $\mathbf{p}_u$ and $\mathbf{r}_u$ can be obtained using a linear complementarity problem (LCP) solver that is able to solve the following linear system:

$$\begin{cases} \mathbf{p}_u = [L_{uu}]\mathbf{r}_u + \mathbf{q}_u \\ \mathbf{p}_u \geq 0 \\ \mathbf{r}_u \geq 0 \\ \mathbf{p}_u{}^T \cdot \mathbf{r}_u = 0 \end{cases} \tag{6}$$

where

$$\begin{aligned}\left[L_{uu}\right] &= -\left[A_{uu}\right]^{-1}\left[B_{uu}\right] \\ \mathbf{q}_u &= -\left[A_{uu}\right]^{-1}\left(\left[A_{uk}\right]\mathbf{p}_k + \left[B_{uk}\right]\mathbf{r}_k + \mathbf{c}_u\right)\end{aligned} \tag{7}$$

3.3 Turbulence problem

Turbulence can occur in the bearings of the last stand of the steel roll forming machine that operate at high speed. In general, its effect is a slight increase in the maximum pressure in the oil-film. In this study, was simply considered by means of Ng and Pan model by considering the coefficients k_x and k_z in eq. (2):

$$\begin{aligned}k_x &= 12 + 0.0136 \cdot Re^{0.9} \\ k_z &= 12 + 0.0043 \cdot Re^{0.96}\end{aligned} \tag{8}$$

where Re is the Reynolds number assumed in the equations. The three flow regimes are delimited by the two well-known Reynolds numbers, namely, $Re_1 = 800$ and $Re_1 = 1500$. The Reynolds number is then evaluated as a function of the local Reynolds number $Re_h = h\rho u / \mu$ as listed in Table 1, where the coefficients a_i for the transitional flow regime allow the continuity of Re and of its first derivative:

$$\begin{aligned}a_0 &= -2(Re_1^2 Re_2^2)/(Re_1 - Re_2)^3 \\ a_1 &= Re_1(Re_1 Re_2 + 4Re_2^2 + Re_1^2)/(Re_1 - Re_2)^3 \\ a_2 &= -2(Re_1 Re_2 + Re_2^2 + Re_1^2)/(Re_1 - Re_2)^3 \\ a_3 &= (Re_1 + Re_2)/(Re_1 - Re_2)^3\end{aligned} \tag{9}$$

Table 1. Flow regime and range of Reynolds number

Flow regime	Range of local Reynolds number Re_h	Reynold number
Laminar	$Re_h \le Re_1$	$Re = 0$
Transitional	$Re_1 \le Re_h \le Re_2$	$Re = a_0 + a_1 Re_h + a_2 Re_h^{\,2} + a_3 Re_h^{\,3}$
Turbulent	$Re_h \ge Re_2$	$Re = Re_h$

3.4 Thermal problem

The distribution of the temperature in the entire bearing is obtained by means of a three-dimensional thermal model that includes a portion of the shaft (S), the oil-films (O) and the bearing (B). Because of the presence of the two axial grooves, the bearing is considered as a two-lobes bearing, neglecting the circumferential groove because of the complexity of such modelling. Regardless, this approximation can be acceptable, considering that the circumferential groove is placed in the unloaded part of the bearing, in which the pressure is quite negligible, and the shear stresses are mainly caused by the Couette flow. Therefore, two oil-film bodies are considered in the model.

The energy equation for each oil-film is as follows:

$$\rho c_p \left(u\frac{\partial T}{\partial x} + v\frac{\partial T}{\partial y} + w\frac{\partial T}{\partial z} \right) = k_{OIL} \left(\frac{\partial^2 T}{\partial x^2} + \frac{\partial^2 T}{\partial y^2} + \frac{\partial^2 T}{\partial z^2} \right) + \mu \left[\left(\frac{\partial u}{\partial y} \right)^2 + \left(\frac{\partial w}{\partial y} \right)^2 \right] \qquad (10)$$

where c_p and k_{OIL} are the heat capacity and the thermal conductivity of the oil, respectively.

The energy equation (10) is valid for laminar flow. For the case considered in the paper the turbulence effect is quite negligible and it has been considered for the evaluation of the pressure distribution. In case of turbulent flow, all the terms in eq. (10) can be seen as the sum of an average value and a fluctuation term.

The use of a two-dimensional thermal model based on the assumption of adiabatic conditions at shaft and bearing surfaces and constant oil temperature in the oil-film thickness can lead to the overestimation of the temperature in the oil-film, especially in the case of bearings operating at high speeds, where shear stresses may be very high. Therefore, a more accurate three-dimensional model must be adopted for the temperature distribution [30]. As a result, the temperature distributions in the bearing and shaft at steady state are governed by the following equations:

$$\begin{aligned} -\nabla\left(k_{BRG}\nabla T\right) &= 0 \\ -\nabla\left(k_{SHAFT}\nabla T\right) &= 0 \end{aligned} \tag{11}$$

where k_{BRG} and k_{SHAFT} are the thermal conductivity coefficients of the bearing and shaft, respectively.

Equations (10) and (11) have been solved by means of the finite element approach using a structured mesh for the oil-films and unstructured meshes for the bearing and shaft, as shown in Fig. 4, for the front bearing of the upper spindle in the first stand, where the oil-film have been magnified in the radial direction. The presence of a portion of the shaft of length equal to approximately three times the length of the bearing allows the heat exchange of the shaft to be considered with a good approximation. The bearing part is composed of the simplified shape of the bearing shown in Fig. 3 and the ring representing

a portion of the bearing housing in the real machine (see, for example, the picture of the bearing assembly in Fig. 12 described in the section of experimental tests). Steel was assumed to be the material for the bearing and shaft parts.

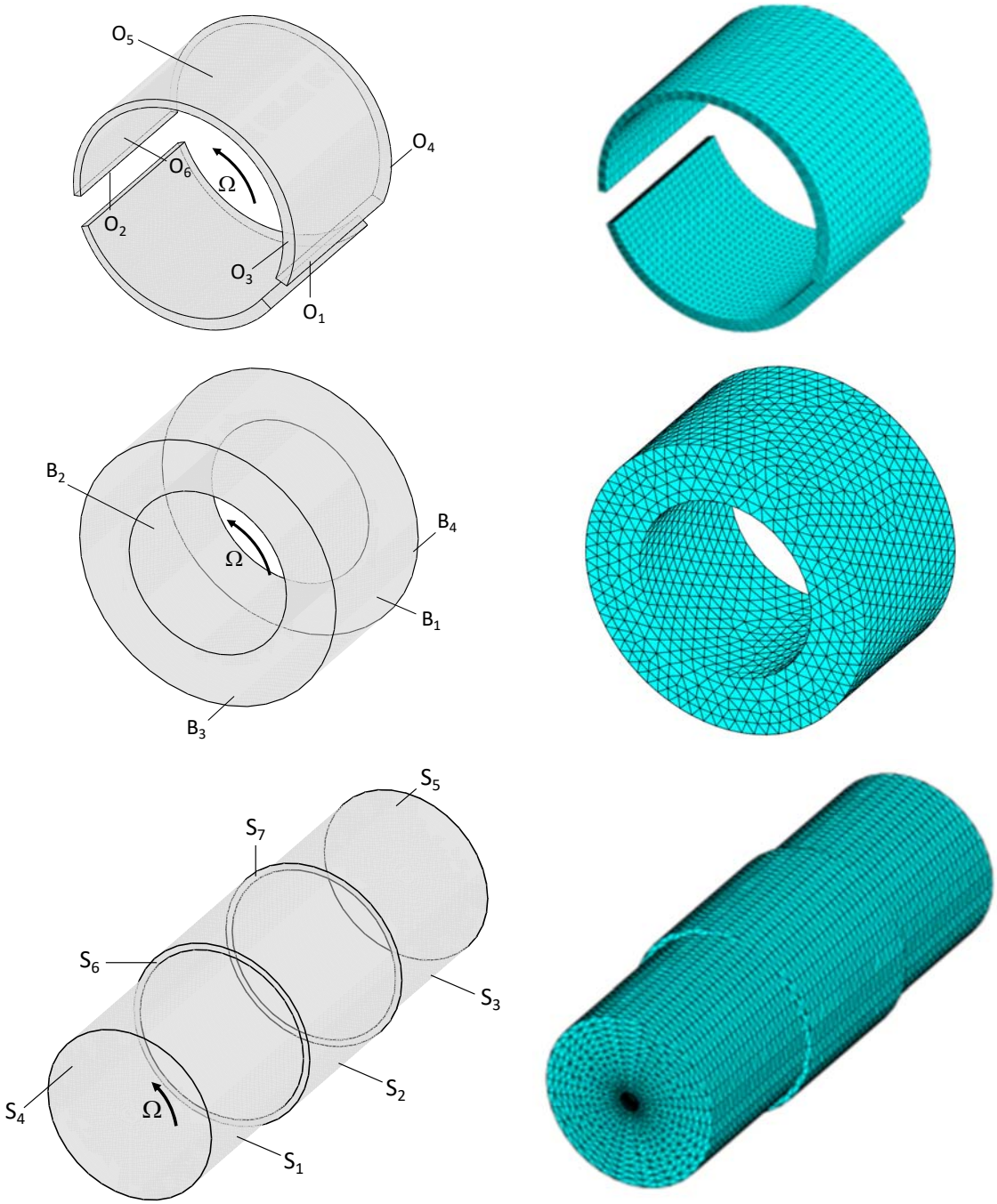

Fig. 4. Bodies and meshes of the thermal model.

The boundary conditions (BC) applied to the faces of the bodies of the model are listed in Table 2.

Table 2. Boundary conditions of the thermal model.

REGION	BC #	FACE #	DESCRIPTION	BC TYPE
k-th OIL PART	**1**	O1	Oil inlet	Fixed temperature @ oil inlet temperature
	2	O2	Oil outlet	Convection with oil @ supply oil temperature
	3	O3	Lateral	Convection with oil @ supply oil temperature
	4	O4	Lateral	Convection with oil @ supply oil temperature
	5	O5	**Bearing interface**	Heat flux from bearing
	6	O6	**Shaft interface**	Temperature from shaft (axial distribution)
BEARING	**7**	B1	External surface	Convection with oil @ supply oil temperature
	8	B2	**Oil interface**	Temperature from oil parts
	9	B3	Lateral	Convection with oil @ supply oil temperature
	10	B4	Lateral	Convection with oil @ supply oil temperature
SHAFT	**11**	S1	Cylindrical	Convection with air @ room temperature
	12	S2	**Oil interface**	Heat flux from oil parts (axial distribution)
	13	S3	Cylindrical	Convection with air @ room temperature
	14	S4	Lateral	Fixed temperature @ supply oil temperature
	15	S5	Lateral	Fixed temperature @ supply oil temperature
	16	S6	Lateral	Convection with oil @ supply oil temperature
	17	S7	Lateral	Convection with oil @ supply oil temperature

The bodies of the model are connected at interfaces, where the temperature and the heat flux of two adjacent bodies must be the same. By considering the *k*-th oil-film body, the conditions are (see Fig. 5):

$$\begin{aligned} T_{O_{5,k}} &= T_{B_{2,k}} \\ \dot{Q}_{O_{5,k}} &= \dot{Q}_{B_{2,k}} \\ T_{S_{2,k}} &= T_{O_{6,k}} \\ \dot{Q}_{S_{2,k}} &= \dot{Q}_{O_{6,k}} \end{aligned} \tag{12}$$

where the heat flux density $\dot{q} = k\nabla T$ is given by:

$$\begin{aligned} \dot{q}_O &= k_O \nabla T \\ \dot{q}_B &= k_B \nabla T \\ \dot{q}_S &= k_S \nabla T \end{aligned} \tag{13}$$

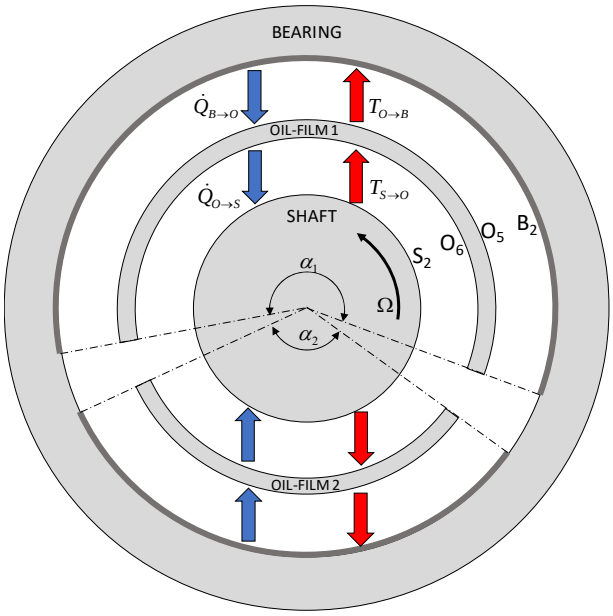

Fig. 5. Boundary conditions at the interfaces.

For the interface between the bearing and the oil-film parts (faces $O_{5,k} - B_2$ as shown in Fig. 5), the temperature distribution from the *k*-th oil-film surface $O_{5,k}$ is applied to the *k*-th active surface $B_{2,k}$ of the bearing. A linear temperature distribution along the circumferential direction is applied in the non-active remaining parts of the bearing inner surface corresponding to the position of the axial grooves. The linear interpolation in the

groove parts connects the outlet temperature of one oil-film part to the inlet temperature of the other oil-film part. The heat flux from the *k*-th active surface $B_{2,k}$ of the bearing is then applied to the outer surfaces $O_{5,k}$ of each oil-film part:

$$\begin{aligned} T_{O_k \to B_k}(y,\theta) &= T_{O_{5,k}}(y,\theta) \\ \dot{q}_{B_k \to O_k}(y,\theta) &= \dot{q}_{B_{2,k}}(y,\theta) \end{aligned} \tag{14}$$

Similar conditions are assumed at the interface between the shaft and the oil-film parts. By considering the rotation of the shaft, a constant temperature along the circumferential direction of the shaft can be assumed. The average temperature along the circumferential direction of the shaft surface S_2 is applied to the inner surface $O_{6,k}$ of each oil-film part. A constant and averaged heat-flux from the inner surfaces $O_{6,k}$ of each oil-film part is then applied to the external surface S_2 of the shaft.

$$\begin{aligned} T_{S \to O_k}(y) &= \frac{1}{2\pi}\int_0^{2\pi} T_{S_2}(y,\theta)\,d\theta \\ \dot{q}_{O \to S}(y) &= \frac{1}{2\pi}\sum_{k=1}^{2}\int_0^{\alpha_k} \dot{q}_{O_{6,k}}(y,\theta)\,d\theta \end{aligned} \tag{15}$$

Furthermore, the inlet temperature $T_{IN,k}$ of each oil-film part was simply evaluated by considering the mixing of the supply oil at the cold supply temperature T_s and the outlet hot oil from the previous oil-film part at temperature $T_{OUT,k-1}$ by means of the “hot-oil carry over” coefficient m:

$$T_{IN,k} = m \cdot T_{OUT,k-1} + (1-m) \cdot T_S \tag{16}$$

where $T_{OUT,k-1}$ represents the average temperature of the oil at the trailing edge of the previous oil-film part.

The solution of the thermal model is obtained by iterating the solution of each subsystem until the convergence criteria based on the relative iteration error of interface conditions is reached. A smooth function between consecutive iterations was adopted on the boundary conditions at interfaces to reduce the oscillations of the numerical solution.

3.5 Lubricant model

The viscosity of lubricating oil is influenced by the temperature T and the pressure p. Furthermore, multigrade engine oils with additives as viscosity index improvers show a shear thinning, that is the non-Newtonian behaviour of the oil which viscosity decreases with the increase in the shear rate $\dot{\gamma}$. In general, the so-called Vogel/Barus/Cross equation for the dynamic viscosity $\mu(T, p, \dot{\gamma})$ can be adopted [31, 32]:

$$\mu(T, p, \dot{\gamma}) = A \cdot \exp\left(\alpha \cdot p + \frac{B}{T+C}\right) \cdot \left(r + \frac{1-r}{1+(K \cdot \dot{\gamma})^m}\right) \tag{17}$$

where α is the piezoviscous coefficient and r, m, K are coefficients representing the viscosity shear thinning.

All the coefficients in eq. (17) depend on the oil type and additives that may not be known in advance. The experimental kinematic viscosity and density as a function of the temperature, are available only for the reference oil.

It is common to assume that the effect of the pressure on the dynamic viscosity for industrial oils is significant for pressures higher than 500-1000 bar. The maximum estimated pressure in the bearings of the steel roll forming machine is about 300 bar and is reached in a small portion (see Fig. 8) of the bearing of the first stand that operates at high load, low speed and low temperature. It is possible to assume that the error in the estimation of the local viscosity can be not negligible but the effect on the power loss can be negligible.

In general, the contribution of the shear thinning to the oil viscosity is more evident for oils with additives. A standard mineral oil is employed in the machine. The shear rate can be estimated to be less than $1 \cdot 10^5 \, 1/s$ and is quite the same for all the bearings in the steel roll forming machine because both the speed (Fig. 2) and the minimum oil-film thickness (Fig. 7c) increase from the first to the last stand.

Therefore, also by considering the parametric analysis that will be shown later for the definition of a new oil formulation only the temperature dependence of oil viscosity has been considered in the paper. The analysis for the reduction of power losses is not performed in absolute terms but in relative terms, in comparison to the reference oil, therefore the error introduced in the estimation of the viscosity can be neglected.

Furthermore, Walther's viscosity model [6] was used for the evaluation of the kinematic viscosity k_ν of the lubricant as the function of the temperature T instead of common Vogel's formula:

$$k_v(T) = \exp\left[\exp\left[A - B\ln(T)\right]\right] - 0.7 \tag{18}$$

The knowledge of the kinematic viscosity of the oil at 40 °C ($kv_{40°C}$) and 100 °C ($kv_{100°C}$) allows the two constants A and B to be evaluated as:

$$B = \frac{\ln\left(\frac{\ln(kv_{100°C}+0.7)}{\ln(kv_{40°C}+0.7)}\right)}{\ln\left(\frac{T_{100°C}}{T_{40°C}}\right)}$$
$$A = \ln\left(\ln(kv_{40°C}+0.7)\right) - B\cdot\ln(T_{40°C}) \tag{19}$$

The normalized kinematic viscosity and density curves as a function of the temperature are shown in Fig. 6 for the reference oil, where all the data are normalized with respect to the corresponding values at 40°C. In Fig. 6 it is possible to observe the good fitting between Walther curve (obtained from 40°C and 100°C points), and the experimental points in the range 40-100°C, where the maximum relative error is about 5% at 60°C.

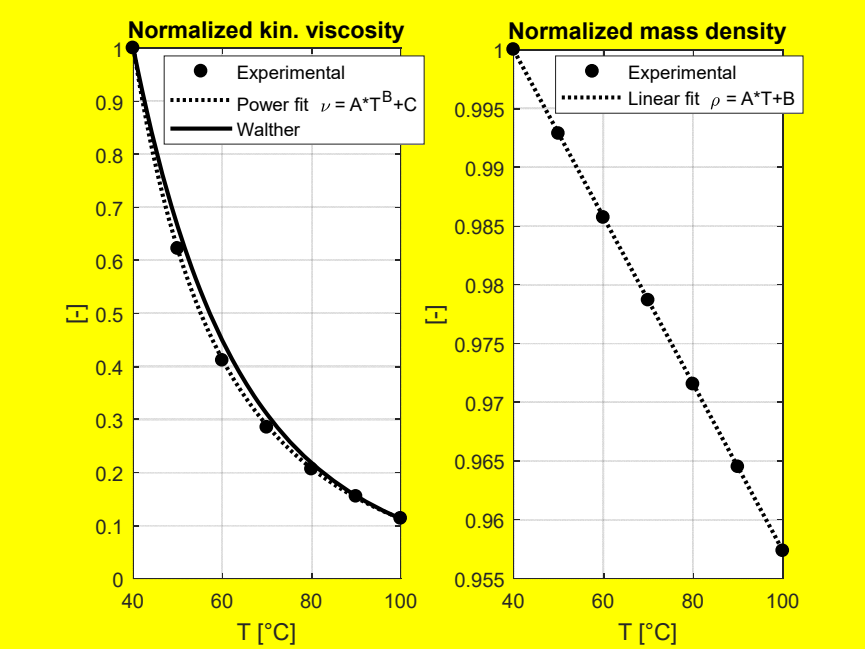

Fig. 6. Normalized viscosity and density curves for the reference oil.

Mass density ρ and specific heat capacity c_p are also given as follows:

$$\rho(T) = C - D \cdot T$$
$$c_p(T) = E + F \cdot T \qquad (20)$$

where C, D, E, F are all positive constants.

By considering the type of analysis that will be shown later for the definition of a new oil formulation, the use of the simple Walther oil model allows an easy interpretation of the results being the temperature behaviour of the oil completely defined by only the two values of the kinematic viscosity at 40 °C and 100 °C.

The temperature distribution in the oil-film parts obtained by the thermal model is then used for the evaluation of the average value of viscosity $\mu = \mu(T)$ and density $\rho = \rho(T)$ in the oil-film to be used in equation (2).

3.6 Bearing deformation

The effect of the deformation of the bearing caused by the pressure distribution and thermal stresses was considered and evaluated by means of a finite element model. The resultant deformation of the bearing surface was transformed in the change of the oil-film thickness.

By considering an isotropic material, the deformation of the bearing (displacement vector **u**) caused by thermal and mechanical stresses is governed by the elasticity equation:

$$-\nabla\left(C \otimes \nabla \mathbf{u}\right) = \frac{E}{1-2\nu}\alpha_t \nabla T \tag{21}$$

where C is the tensor of mechanical properties, α_t the thermal expansion coefficient, E the Young's modulus, and ν the Poisson's ratio of the material.

Additional boundary conditions are applied on all surfaces of the bearing to consider the equivalent traction stresses for the evaluation of the thermal deformation.

4 Results for the reference oil

The bearings of the steel roll forming machine operate in a wide range of conditions in terms of load and rotational speed. The bearings in the first stage run at low speed and high load, whereas the bearings in the last stand operate at high speed and low load (see Fig. 2).

By considering the reference oil, the behaviour of all the 40 bearings in the steel roll forming machine was simulated by assuming the same supply conditions of the oil for all the bearings that, for this application, are typically represented by the temperature of 30÷50°C and feeding pressure of 0.1÷0.5 MPa.

The maximum power loss and the maximum oil-film temperature are obtained, as expected, in the front bearing of the last stands that runs at high speed, as shown in Fig. 7, in which all the values were normalized with respect to the maximum corresponding value. The temperature in Fig. 7b was normalized by considering the original temperatures expressed in °C.

The total power loss in the bearings of the forming machine can be evaluated as:

$$P_{loss} = 2\sum_{u=1}^{N}\sum_{b=1}^{2}\int_{dA}\Omega_u R_b \tau_{shaft}\, dA \tag{22}$$

where Ω_s is the rotational speed of the *u*-th stand, R_b is the radius of the *b*-th bearing (front and rear), and τ_{shaft} is the shear-stress on the shaft.

The maximum temperature is obtained, as expected, in the front bearing of the last stands that runs at high speed.

Conversely, the minimum oil-film thickness is obtained in the front bearing of the first stand of the machine that operate at the maximum load, as shown in Fig. 7c, where the minimum oil-film thickness was normalized with respect to the maximum value obtained in the last stand.

Therefore, from this analysis, it appears possible to reduce the power loss in the bearings of the forming machine mainly by adopting a new oil with lower viscosity.

Conversely, the design of the new oil must consider a trade-off between the reduction of power loss in the last stands and the limit on the minimum oil-film thickness reached in the first stands of the machine; this trade-off must be carefully investigated.

In eq. (22) it is assumed that only hydrodynamic losses occur in the lubricant, that is no mixed lubrication or friction due to asperity contact between sliding surfaces takes place.

The reduction of the oil viscosity will lead to a reduction of the oil-film thickness. Therefore, it is necessary to evaluate the permissible value of the minimum oil-film thickness under which mixed lubrication and wear can occur.

According to standard ISO 7902-3, the permissible value of minimum oil-film thickness $h_{\lim}$ for plain journal bearings can be determined from the following equation:

$$h_{\lim} = Rz_B + Rz_J + \frac{1}{2}By + \frac{1}{2}y + h_{wav,eff} \qquad (23)$$

Eq. (23) takes into account the sum of the mean peak-to-valley heights (roughness) of the bearing (Rz_B) and the journal (Rz_J), the misalignment within the bearing length ($\frac{1}{2}By$), the mean deflection ($\frac{1}{2}y$) and the effective waviness in circumferential direction.

The arithmetical mean roughness for the shaft and the bearing can be extracted by the design specifications and are equal to $Ra_J = 0.2\mu m$ and $Ra_B = 0.4\mu m$ that correspond roughly to mean roughness $Rz_J = 0.8\mu m$ and $Rz_B = 1.6\mu m$. By considering only the

effect of roughness, the minimum oil-film thickness can be estimated as $h_{\lim} = 2.4\mu m$. The same standard ISO 7902-3 provides a table with empirical permissible values as a function of shaft diameter and sliding velocity of the shaft, in which a mean peak-to-valley height of $Rz_J \leq 4\mu m$ for the shaft, minor geometrical errors of the sliding surfaces, careful assembly and adequate filtering of the lubricant are assumed. For the case considered in the paper, this empirical value is $h_{\lim} = 12\mu m$.

Another approach for the evaluation of the permissible value of minimum oil-film thickness is based on the use of the Greenwood and Tripp contact model [16, 18]. The friction force caused by asperity contact depend on the asperity contact pressure $p_a = K \cdot E^* \cdot F_{5/2}(H_s)$ where H_s is a dimensionless clearance parameter. The expression of the form function $F_{5/2}(H_s)$ states that the friction force is null for $H_s \geq 4$. Therefore, this condition can be assumed as lower limit for the oil-film thickness:

$$h_{\min} \geq 4\sigma_s + \overline{\delta}_s \tag{24}$$

where σ_s is the combined asperity summit roughness and $\overline{\delta}_s$ is the combined mean summit height. These last two quantities can be evaluated by experimental measurement of the bearing and shaft surface profiles.

a)

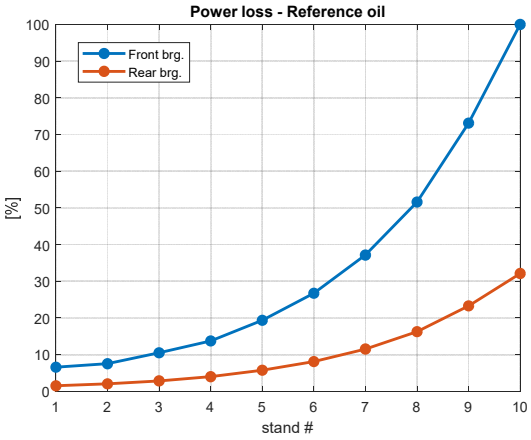

b)

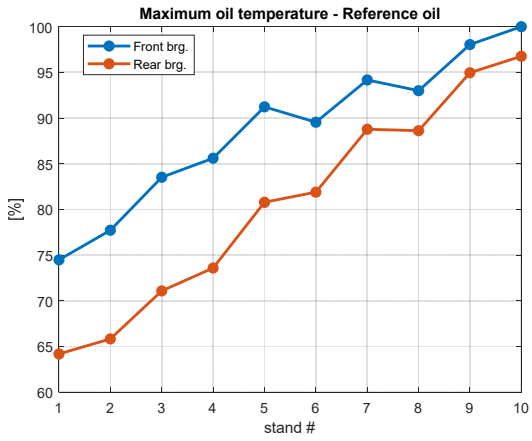

c)

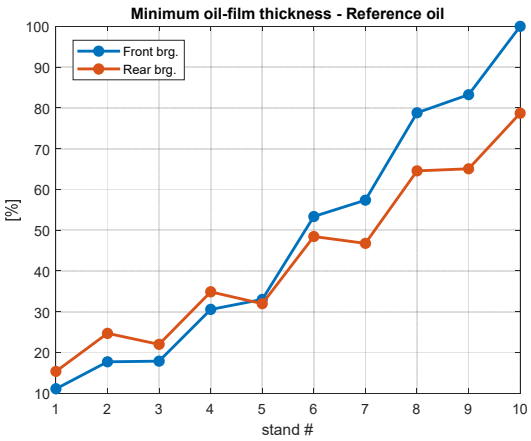

Fig. 7. Power losses a), maximum temperature b) and minimum oil-film thickness c) in the bearings for the reference oil.

For the sake of brevity, only the results of the front bearings of the upper spindles for the first and last stands are shown in the following. The pressure and temperature distributions for the reference oil are shown in Fig. 8 and Fig. 9 for the first and last stand, respectively, and the corresponding bearing deformations are shown in Fig. 10. The colours in the pressure distribution in Fig. 8b and Fig. 8c range from blue to red, with blue and red corresponding to the minimum and maximum value obtained in each individual simulation, respectively.

In Fig. 9, the oil-film parts are magnified, and the colour range is the same for both the first and the last stands. The same scale factor is used for the deformations in Fig. 10a and Fig. 10b.

Large oil-film pressure and non-negligible bearing deformations are obtained in the bearing of the first stand that operate at high load. Conversely, the maximum temperature is obtained in the last stand, which operates at the maximum speed and where high shear stresses occurred.

The maximum radial deformation of the bearing in Fig. 10 for the first stand is of the same order of magnitude of the minimum oil-film thickness and therefore cannot be neglected. Conversely, the maximum radial deformation of the bearing of the last stand is one order of magnitude lower than that of the first stand.

For the bearing in the first stand and the reference oil, an overestimation of about 28% occurs in the maximum pressure of the oil-film if simple Gumbel's boundary condition is used and if the bearing deformation is neglected. By considering the LCP method for the pressure distribution, the effect of the bearing deformation can be estimated in a reduction of the maximum pressure of about 12%.

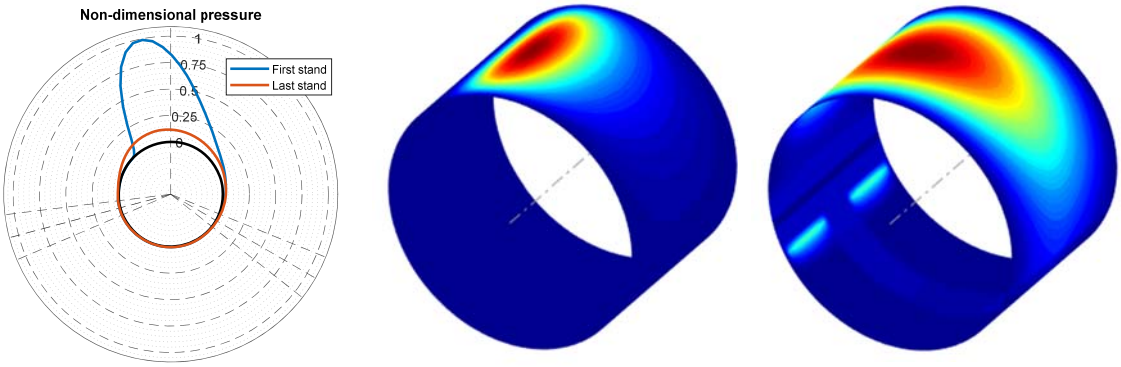

a) b) c)

Fig. 8. Pressure distributions: a) comparison between first and last stands in the cross section, b) 3D for first stand and c) 3D for last stand.

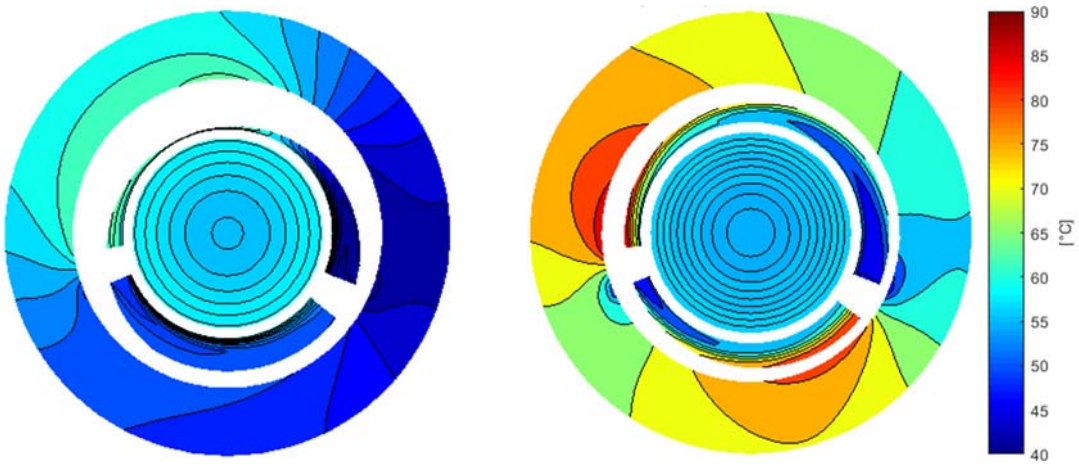

a) b)

Fig. 9. Temperature distributions in the cross section (middle plane) of the bearing for the first stand (a) and last stand (b) using the same colour range.

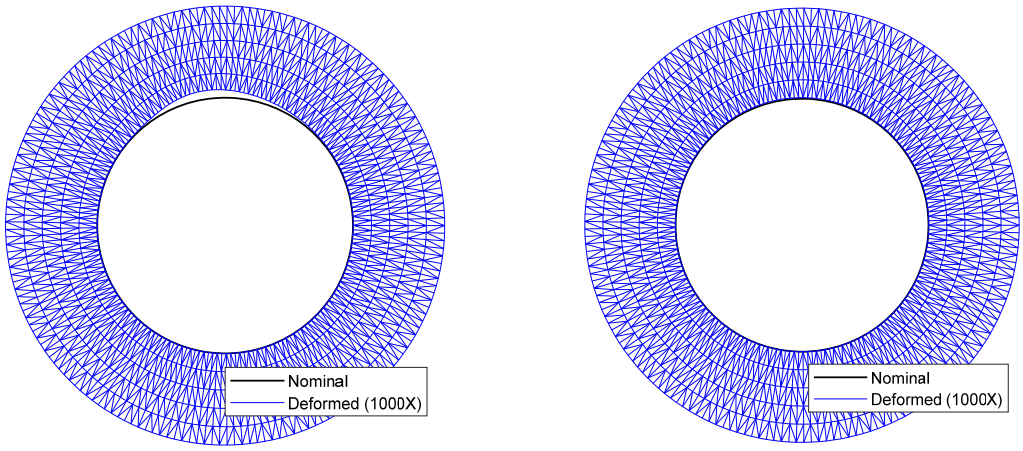

a) b)

Fig. 10. Bearing deformations in the cross section (middle plane) of the bearing for the first stand (a) and the last stand (b).

5 Characteristics of the new oil

In this section, the behaviours of all the bearings of the machine were investigated for different oil properties defined by the two kinematic viscosities kv at 40°C and 100°C. The percentage variation of the power loss with respect to the reference oil, that is the actual oil used in the forming machine, is shown in Fig. 11a, in which the black dot represents the reference condition. The kinematic viscosities of the oils were normalized to the viscosity of the reference oil. The range of analysis for the kinematic viscosity at 40°C is approximately 45-120% of the viscosity of the reference oil (horizontal axis of and Fig. 11a) and a range of 20-115% is considered for the kinematic viscosity at 100°C (vertical axis of and Fig. 11a). In Fig. 11a, note that the highest power loss reduction can be obtained by reducing the viscosity of the oil. For example, by using an oil defined by

the lower values of the range of analysis (bottom-left corner of Fig. 11a), a reduction of approximately 45% of the power for the reference oil can obtained. This reduction could appear trivial if considered in general, but the analysis of Fig. 11a shows that the power loss does not follow a linear mode. However, the two viscosity parameters $kv_{40°C}$ and $kv_{100°C}$ are not independent themselves. Real oils show a behaviour represented by a limited range of viscosity index that relates the two kinematic viscosities. The dashed black line in Fig. 11a represents the typical behaviour of industrial oils.

Conversely, the reduction of the oil viscosity leads to a reduction of the minimum oil-film thickness, as shown in Fig. 11b. The value of the minimum oil-film thickness is critical for the bearings in the first stand that operate at high load and low speed.

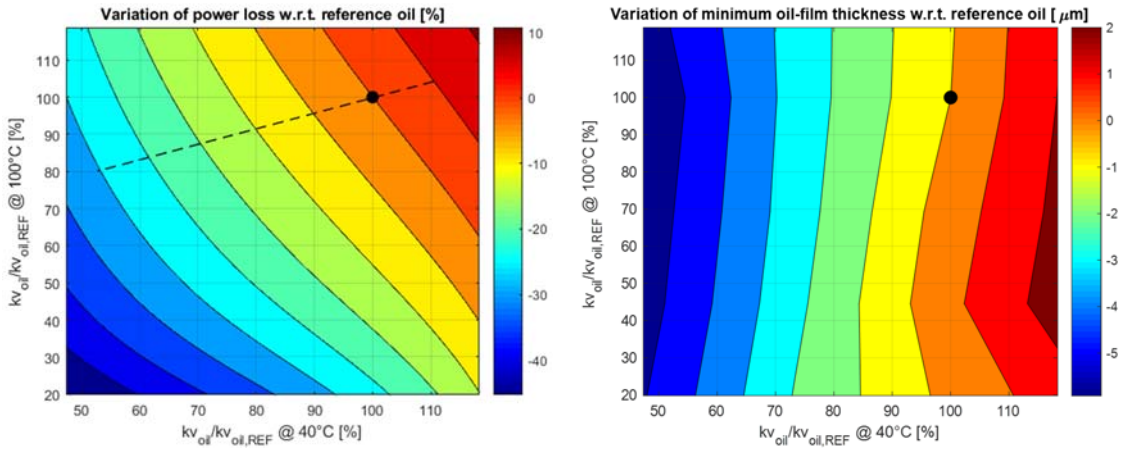

a) b)

Fig. 11. Variation of a) power loss and b) minimum oil-film thickness with respect to the reference oil.

6 Experimental tests

The previous analysis shows that it is possible to obtain a reduction of approximately 20-30% of the power loss in the bearings of the forming machine, corresponding to several tens of kilowatts, by reducing the viscosity of the lubricant.

An experimental activity was performed using a test rig equipped with a bearing having similar dimensions to those of the front bearings of the machine described in the paper [7]. Experimental tests were performed to evaluate the behaviour of the bearing and the reduction of the power loss for two different oils, the current one used in the real machine, and a new oil with lower viscosity, approximately half of the reference one.

6.1 Test rig description

The main components of the test rig are a rigid shaft driven by a 15-kW motor through a flexible coupling and able to rotate to the maximum speed of 1465 rpm. The shaft is supported by two rolling element bearings at the two ends of the shaft that rotates in counter-clockwise direction from the non-driven end (NDE) view. The vertical load is applied on the top of the bearing case through two hydraulic actuators with the maximum available force of 400 kN. The vertical load acting on the housing support is in the downward direction corresponding to a load applied on the shaft in the upward direction (Fig. 12).

The bearing, which is centrally placed on the rotating shaft, has the nominal diameter of 160 mm and length of 145 mm. The bearing is equipped with 9 temperature probes (T1 to T9 in Fig. 12) and 3 pressure probes (P1, P2 and P3 in Fig. 12) both placed in the loaded part of the bearing, whereas the relative position of the shaft with respect to the bearing is monitored by 2 proximity probes (XC and YC in Fig. 12).

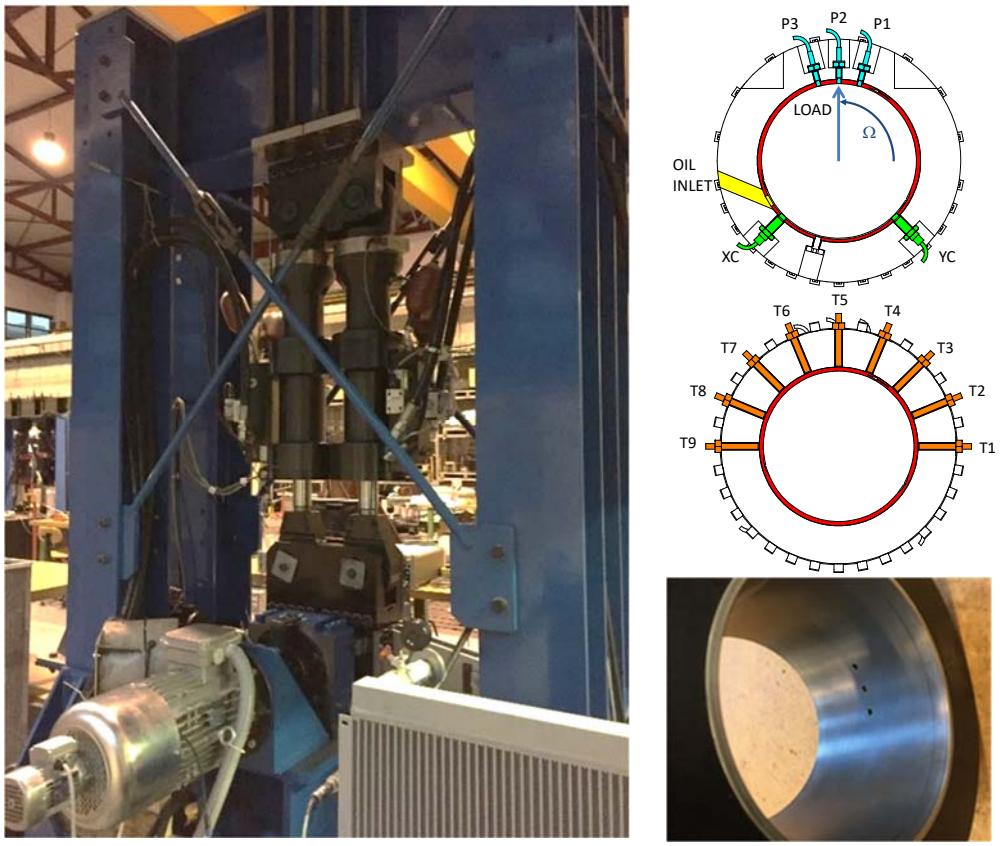

Fig. 12. Picture of the test rig, position of the sensor in the bearing and picture of the holes of the pressure probe in the loaded part of the bearing.

6.2 Experimental results

The tests of the two oils were performed using the same operating conditions: supply oil temperature at 40 °C, supply oil pressure at 2.5 bar and rotational speed of 1200 rpm. The tests performed for the reference oil were repeated without any system modification by simply changing the oil in the lubricating circuit. As already stated, the new oil has a viscosity of approximately half of the reference oil. The static and dynamic behaviour of

the bearing was investigated by applying a load in the range of 40-180 kN. The procedure for the evaluation of the dynamic coefficients is the same as that described in [7].

The behaviour of the bearing operating with the two oils shows the increase in the temperature as function of the increase of the load (Fig. 13). The maximum temperature, measured by probe T7, is approximately 7 °C lower for the new oil because of the lower shear stresses caused by the lower viscosity of the new oil than the reference one.

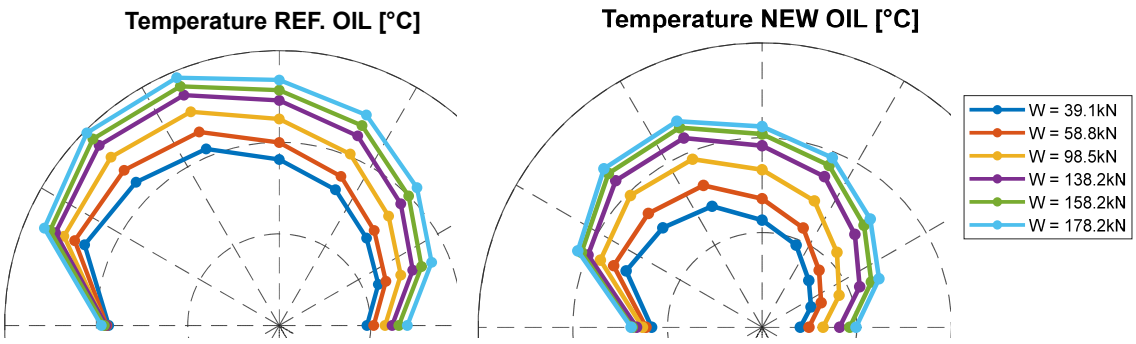

Fig. 13. Experimental temperature distribution for the two oils.

By increasing the load in the upward direction, the static position of the shaft moves in the upward direction, as shown in Fig. 14a, where the position of the shaft has been normalized with respect to the maximum position for the reference oil in vertical direction. The difference between the static centre positions for the two oils is approximately 7-8 μm in the vertical direction. Because the bearing used in the tests the same for the two oils, and considering the position of the minimum oil-film thickness provided by a model, it is possible to estimate a reduction in the oil-film thickness lower than 7-8 μm for the new oil.

The shaft centre position for the new oil is cross checked by the analysis of the pressure measured by the fixed pressure probes. By considering Fig. 12 and the direction of shaft rotation, the pressure distribution shows a maximum close to the position of pressure probe P3. By increasing the load, the pressure measured by the three probes increased for both oils, as shown in Fig. 14b. From Fig. 14b it is possible to observe the light reduction of the pressures P1 and P3 and the increase of pressure P2 for the new oil with respect to the reference one.

The reduction of the oil-film thickness is eventually confirmed by the increase of the dynamic stiffness coefficient Kyy in the direction of the load for the new oil, as shown in Fig. 14c.

a)

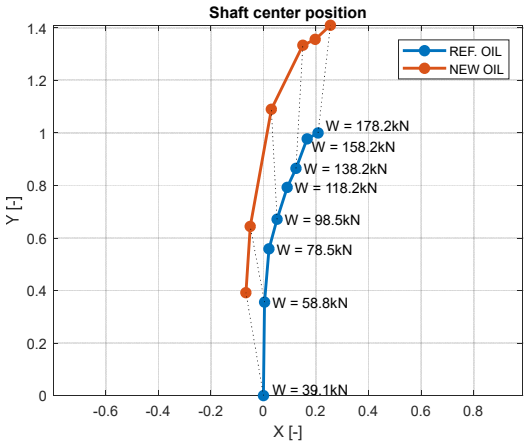

b)

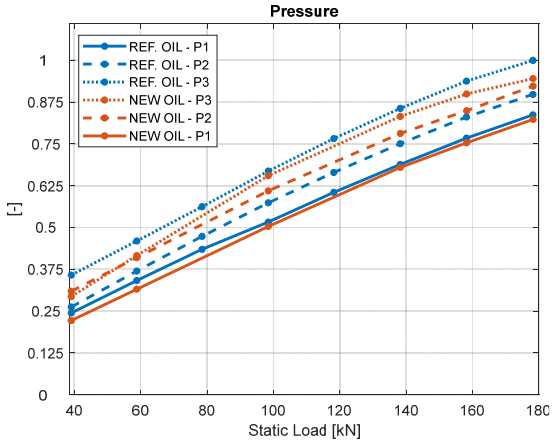

c)

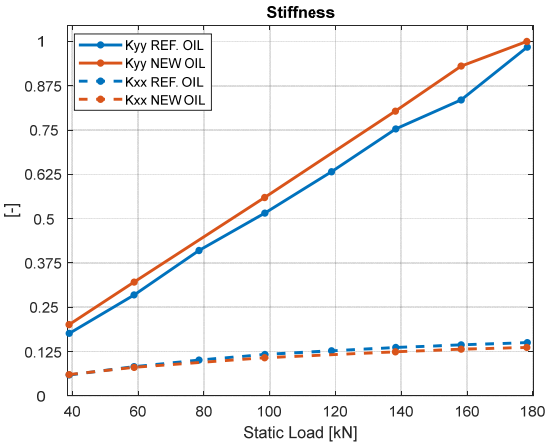

Fig. 14. Experimental shaft centre position a), pressures b) and stiffness coefficients c) for the two oils.

The power loss in the bearing has been evaluated by means of the motor current provided by the inverter of the motor and knowing the current constant K_I of the motor that allow the evaluation of the motor torque. The total torque given by the motor includes the shear stresses in the oil-film, the friction in the two rolling element bearings that support the shaft, and the dissipation of the motor itself. Therefore, it is assumed that, for two different oils, all the dissipations are the same except the effect of the viscosity in the shear stresses of the oil-film bearing.

The friction torque $M_{friction}$ of the two rolling element bearings (SKF 24030) was evaluated by means of formulas provided by bearing manufacturer. The friction torque is given by the sum of the torque M_0, which is independent of the load, and the component M_1, which is a function of the load:

$$\begin{aligned} M_{friction} &= M_0 + M_1 \\ M_0 &= 10^{-7} f_0 \left(\nu \cdot n\right)^{2/3} {d_m}^3 \\ M_1 &= f_1 \cdot P_1^a \cdot {d_m}^b \end{aligned} \tag{25}$$

where $f_0 = 6.5$ is a coefficient that is a function of bearing and lubrication type, $f_1 = 0.0008$ is a coefficient that is a function of bearing and load type, $a = 1.5,\ b = -0.2$ coefficients are each a function of the bearing type, $n = 1200\text{rpm}$ is the rotational speed, $d_m = 0.5\left(d + D\right) = 187.5\text{mm}$ is the pitch diameter of the rolling element bearing, $\nu = 15\,\text{mm}^2/\text{s}$ is the kinematic viscosity of the ISO-VG46 oil at 70 °C used for the lubrication of the rolling element bearings, and P_1 is the load acting on each rolling element bearing (half of the load applied to the oil-film bearing).

By subtracting the friction torque of the two rolling element bearings from the motor torque, it is possible to obtain the power loss of the oil-film bearing for the reference and the new oils.

By using the fitting curves of the power loss for the reference and the new oils, the percentage reduction of power loss with respect to the reference oil can be evaluated as:

$$\Delta P_{loss}\% = \frac{P_{REF.OIL} - P_{NEW\,OIL}}{P_{REF.OIL}} \cdot 100 \tag{26}$$

The power loss reduction is a function of the load and can be estimated as approximately 21-27% in the load range investigated in the experimental tests, as shown in Fig. 15.

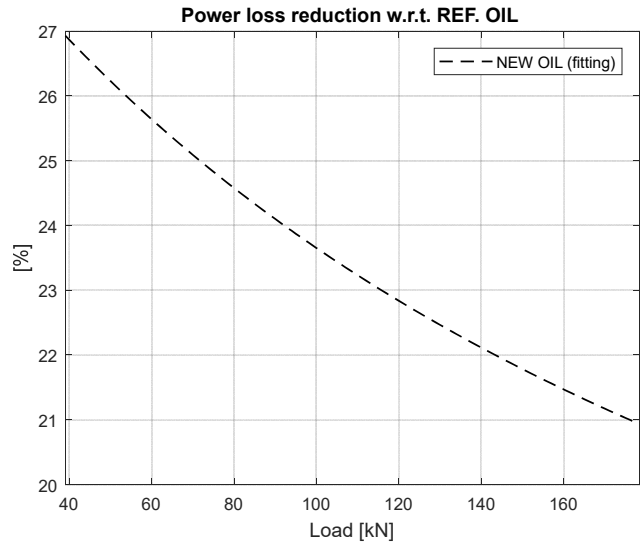

Fig. 15. Estimation of power loss reduction of the new oil w.r.t. the reference oil.

7 Conclusions

The reduction of the total power loss caused by shear stresses in the oil-film bearings of a steel roll forming machine was investigated in this paper.

The analysis was performed by simulating the behaviour of all the bearings by means of an accurate TEHD model. The machine studied uses the same lubricant for all the bearings; furthermore, the machine is equipped with the same bearings for all the stands. Therefore, the bearings operate in a wide range of loads and speeds. The result is that the maximum power loss is obtained in the bearings operating at high rotational speed. Conversely, the minimum oil film-thickness is obtained in the first stand of the machine operating at minimum speed and maximum load. The reduction of the power loss can be obtained by the reduction of the oil viscosity. The results of simulations showed that the overall power loss in the bearings of the forming machine can be reduced of approximately 30% by using an oil with kinematic viscosity of approximately half the value of the reference oil. Moreover, the behaviour of a bearing having similar dimensions and operating in similar conditions of one of the first stands of the machine considered in the simulations was investigated. The reference oil used in the experimental activity was the same oil used in the real machine. Furthermore, an oil having the kinematic viscosity of approximately half the value of the reference oil was tested. In the experimental test, a reduction of the power loss in the range of 20-25% with respect to the reference oil was obtained with the new oil.

References

1. Pennacchi, P. Introduction of advanced technologies for steam turbine bearings. In Tanuma, T. (ed.) Advances in Steam Turbines for Modern Power Plants, Elsevier, Amsterdam; 2016, p. 321-380.
2. Forsthoffer, W.E. Forsthoffer's Best Practice Handbook for Rotating Machinery. Butterworth-Heinemann, Oxford; 2011.
3. Frêne, J., Nicolas, D., Degueurce, B., Berthe, D., Godet, M. Hydrodynamic lubrication – bearing and thrust bearings. Elsevier Science BV, Amsterdam; 1997.
4. Hori, Y. Hydrodynamic lubrication. Springer-Verlag, Tokio; 2006.
5. Someya, T. Journal-bearing databook. Springer-Verlag, Berlin; 1989.
6. Stachowiak, G.W., Batchelor, A.W. Engineering tribology. Butterworth Heinemann, Burington; 2005.
7. Chatterton, S., Dang, P.V., Pennacchi, P., De Luca, A., Flumian, F. Experimental evidence of a two-axial groove hydrodynamic journal bearing under severe operation conditions. Tribology International 2017; 109: p. 416-427. DOI: 10.1016/j.triboint.2017.01.014
8. Wojtkowski, T.C., Osgood, P.N. Development of large, high capacity oil film bearings for steel rolling applications. In: AISTech - Iron and Steel Technology Conference Proceedings Nashville, USA 2004; 2: p. 535-544.
9. Xu, Z., Chen, D. Analyses of the oil film compensation and critical rolling speed for hydrodynamic journal bearing in rolling mill. Run Hua Yu Mi Feng/Lubrication Engineering 1998; p. 4: 41-42+45.
10. Kalpakjian, S., Schimd, S.R. Manufacturing engineering and technology. 7th ed. Pearson College division. 2008.

11. R. Kopp. Some current development trends in metal-forming technology. Journal of Materials Processing Technology 1996; 60(1–4), p. 1-9. DOI: 10.1016/0924-0136(96)02301-1

12. Dickenson, A. Engine friction modelling with consideration of lubricant tribological characteristics, Industrial Lubrication and Tribology 1999; 51(4), p. 223-224.

13. Knauder, C.; Allmaier, H.; Sander, D.; Salhofer, S.; Reich, F.; Sams, T. Analysis of the Journal Bearing Friction Losses in a Heavy-Duty Diesel Engine. Lubricants 2015, 3(2), 142-154; https://doi.org/10.3390/lubricants3020142.

14. Ligier, J.; Noel, B. Friction Reduction and Reliability for Engines Bearings. Lubricants 2015, 3(3), 569-596; https://doi.org/10.3390/lubricants3030569.

15. Carden, P., Pisani, C., Andersson, J., Field, I., Lainé, E., Bansal, J. & Devine, M. The Effect of Low Viscosity Oil on the Wear, Friction and Fuel Consumption of a Heavy Duty Truck Engine, SAE International Journal of Fuels and Lubricants 2013, vol. 6, no. 2.

16. Allmaier, H., Priestner, C., Six, C., Priebsch, H.H., Forstner, C., Novotny-Farkas, F. Predicting friction reliably and accurately in journal bearings - A systematic validation of simulation results with experimental measurements. Tribology International 2011, 44 (10), p. 1151-1160. DOI: 10.1016/j.triboint.2011.05.010

17. Allmaier, H., Priestner, C., Reich, F.M., Priebsch, H.H., Novotny-Farkas, F. Predicting friction reliably and accurately in journal bearings - Extending the EHD simulation model to TEHD. Tribology International 2013, 58, p. 20-28. DOI: 10.1016/j.triboint.2012.08.015

18. Bergmann, P., Grün, F., Gódor, I., Stadler, G. & Maier-Kiener, V. On the modelling of mixed lubrication of conformal contacts, Tribology International 2018, vol. 125, p. 220-236.

19. Sander, D.; Knauder, C.; Allmaier, H.; Damjanović-Le Baleur, S.; Mallet, P. Friction Reduction Tested for a Downsized Diesel Engine with Low-Viscosity Lubricants Including a Novel Polyalkylene Glycol. Lubricants 2017, 5(2), 9; https://doi.org/10.3390/lubricants5020009.
20. Allmaier, H., Priestner, C., Reich, F.M., Priebsch, H.H., Forstner, C., Novotny-Farkas, F. Predicting friction reliably and accurately in journal bearings the importance of extensive oil-models. Tribology International 2012, 48, p. 93-101. DOI: 10.1016/j.triboint.2011.11.009
21. Grützmacher PG, Rosenkranz A, Szurdak A, König F, Jacobs G, Hirt G, et al. From lab to application - Improved frictional performance of journal bearings induced by single- and multi-scale surface patterns. Tribology International 2018;127, p. 500-508.
22. Murthy A.A. and Raghunandana D., Study of Dimple Effect on the Friction Characteristics of a Journal Bearing using Taguchi Method IOP Conference Series: Materials Science and Engineering 2018, Vol. 314, DOI:10.1088/1757-899X/314/1/012014.
23. Kalogiannis K, Merritt DR, Mian O, Morina A, Neville A, Liskiewicz T. Contact and wear thermo-elastohydrodynamic model validation for engine bearings. Proc Inst Mech Eng Part J J Eng Tribol 2017;231(9):1117-1127.
24. Wei, Y., Chen, Z.-., Jiao, Y.-. & Xu, W. Effects of dimensional tolerances on the friction power loss of hydrodynamic journal bearing system" Journal of Donghua University (English Edition), 2014 vol. 31, no. 3, pp. 266-271.
25. Simmons, G.F., Glavatskih, S.B., Synthetic lubricants in hydrodynamic journal bearings: Experimental results, Tribology Letters 2011; 42(1), p. 109-115. DOI: 10.1007/s11249-011-9753-2

26. Gulzar, M., Masjuki, H.H., Kalam, M.A., Varman, M., Zulkifli, N.W.M., Mufti, R.A. & Zahid, R. Tribological performance of nanoparticles as lubricating oil additives, Journal of Nanoparticle Research 2016 , vol. 18, no. 8.

27. Marx, N., Fernández, L., Barceló, F. & Spikes, H. Shear Thinning and Hydrodynamic Friction of Viscosity Modifier-Containing Oils. Part I: Shear Thinning Behaviour,. Tribology Letters 2016, vol. 66, no. 3.

28. Zhang, Z.S., Dai, X.D. & Xie, Y.B. 2013, "Thermoelastohydrodynamic behavior of misaligned plain journal bearings", Proceedings of the Institution of Mechanical Engineers, Part C: Journal of Mechanical Engineering Science, vol. 227, no. 11, pp. 2582-2599.

29. Suh J., Palazzolo A. Three-dimensional dynamic model of TEHD tilting-pad journal bearing - Part I: theoretical modeling. Journal of Tribology 2015; 137(4), p. 1-11.

30. Dang, P.V., Chatterton, S., Pennacchi, P., Vania, A.: Effect of the load direction on non-nominal five-pad tilting-pad journal bearings. Tribology International 2016; 98, p. 197-211.

31. Bukovnik, S., Offner, G., Čaika, V., Priebsch, H.H. & Bartz, W.J. Thermo-elasto-hydrodynamic lubrication model for journal bearing including shear rate-dependent viscosity, Lubrication Science 2007, vol. 19, no. 4, pp. 231-245.

32. Sander, D.E., Allmaier, H., Priebsch, H.H., Reich, F.M., Witt, M., Füllenbach, T., Skiadas, A., Brouwer, L. & Schwarze, H. Impact of high pressure and shear thinning on journal bearing friction", Tribology International 2015, vol. 81, pp. 29-37.

33. Giacopini, M., Foweel, M.T., Dini, D., Strozzi, A. A mass-conserving complementarity formulation to study lubricant films in the presence of cavitation. Journal of Tribology 2010; 132, Article 041702.